PERGAMON

International Journal of Heat and Mass Transfer 44 (2001) 4579–4592

International Journal of HEAT and MASS TRANSFER

www.elsevier.com/locate/ijhmt

Studies of splat morphology and rapid solidification during thermal spraying

H. Zhang [a,*], X.Y. Wang [a], L.L. Zheng [a], X.Y. Jiang [b]

[a] *Department of Mechanical Engineering, State University of New York at Stony Brook, Stony Brook, NY 11794-2300, USA*
[b] *Advanced Materials Technology, Caterpillar Inc., Peoria, IL 61656-1875, USA*

Received 3 November 2000; received in revised form 16 March 2001

Abstract

The splat morphology and substrate melting and re-solidification have been studied numerically and experimentally for molybdenum droplets impacting on molybdenum, mild steel, and glass substrates. The effects of the droplet size, velocity, temperature, and substrate material and temperature on the splat morphology and the rate of solidification have been investigated. The correlation between the splat flattening ratio and the Reynolds and Jakob numbers has been developed. The substrate melting and re-solidification strongly depends on the impinging temperature of the droplet, substrate temperature and its thermophysical properties. A two-dimensional model considering free surface deformation and rapid solidification has been developed and used to predict the splat morphology.

Keywords: Rapid solidification; Thermal spray coating; Materials processing

1. Introduction

Thermal spray processing is a well-established method for forming protective coatings; free standing forms and processed materials. It combines the steps of melting, rapid quenching, and consolidation into a single step, and produces a variety of material characteristics, including fine grain sizes, extended solid solubility, metastable phases, and amorphous phases. The quality of the spray coating is mainly determined by the conditions of the impacting particles such as size, velocity, temperature, and phase, as well as the substrate conditions, such as thermophysical properties, surface roughness, wetting ability, temperature, and contact resistance. It is therefore necessary to develop a good understanding of the fundamental physical principles governing droplet spreading and solidification so that the correlation between the process parameters (gas velocity and temperature, substrate temperature and thermophysical properties, powder size and materials) and the properties of the splats can be established and the coating quality can be controlled.

Many theoretical and experimental studies have been conducted to examine the impact of a molten droplet on a substrate. Madejski [1] developed the first model that could predict the splat-flattening ratio, e.g., the maximum spreading of a molten droplet. The predictions agreed with experimental measurements for tin and lead droplets on a flat plate. Collings et al. [2] studied molten alloy droplets impacting on copper, alumina, and quartz substrates, and found that the splat morphology depended on substrate thermal properties. Many researchers have further improved Madejski's model to include the effects of surface tension, solidification, and thermal contact resistance; and found the splat-flattening ratio a function of the Reynolds, Weber, Prandtl, and Jakob numbers [3–7]. For the splashed splats, Aziz and Chandra [7] investigated the impact, recoil, and solidification of a molten tin droplet on a stainless steel substrate. Based on the Rayleigh–Taylor instability theory, they developed a theoretical model to predict the finger number around

* Corresponding author. Tel.: +1-631-632-8492; fax: +1-631-632-8544.
E-mail address: hui.zhang@sunysb.edu (H. Zhang).

0017-9310/01/$ - see front matter
PII: S0017-9310(01)00109-0

Nomenclature

a	constant
b	reference thickness (m)
Bi_c	Biot number, $Bi_c = h_c d/k_j$
c	specific heat (J kg^{-1} K^{-1})
d	droplet diameter (m)
F	volume of fluid function
f	mass fraction
h	enthalpy (kJ kg^{-1})
h_c	heat transfer coefficient (W m^{-2} K^{-1})
h_f	latent heat (J kg^{-1})
Ja	Jakob number, $Ja = c_s(T_f - T_{sub})/h_f$
k	thermal conductivity (W m^{-1} K^{-1})
P	pressure (Pa)
Pr	Prandtl number, $Pr = v/\alpha$
Ra	Surface roughness (μm)
Re	Reynolds number, $Re = \rho V d/\mu$
r	radial coordinate (m)
St	Stefan number, $St = c_l(T_p - T_f)/h_f$
s	thickness of the deposited layer (m)
T	temperature (K)
t	time (s)
U	reference velocity (m s^{-1})
$\vec{u}$	non-dimensional velocity vector
V	impacting velocity (m s^{-1})
V_i	interface velocity (m s^{-1})
We	Weber number, $We = \rho V^2 d/\sigma_o$
z	axial coordinate (m)

Greek symbols

α	thermal diffusivity (m^2 s^{-1})
θ	non-dimensional temperature
μ	dynamic viscosity (N s m^{-2})
μ_k	linear kinetic coefficient (m s K^{-1})
ξ	flattening ratio
ρ	density (kg m^{-3})
σ	surface tension (N m^{-1})
λ	thermal conductivity ratio, $\lambda = (f_s k_s + f_l k_l)/k_l$
κ	local curvature (m^{-1})

Subscripts

B	bottom of the droplet
c	interface between droplet and substrate
f	fusion
i	solidification interface
l	liquid
m	melting temperature
p	droplet
s	solid
sub	substrate

Superscripts

$*$	dimensional variable

the periphery of the splat. Fukumote and Huang [8] conducted experiments to study splashing phenomena. They discovered that splat morphology changes from splashed to disk-shaped when the substrate temperature reaches a certain value. They have defined this value as the "transition temperature."

Along with theoretical and experimental research, computational studies have been conducted for thermal spray processes. Trapage et al. [9,10] investigated the impact of a lead droplet in the absence of solidification using a three-dimensional code, FLOW-3D. By using a VOF-based computer package, RIPPLE [11], Liu et al. [12,13] studied splat formation and solidification processes, in particular, the interaction between the free surface and solidification interface, and the interaction between two droplets impinging on a pre-determined non-flat surface [13,14]. Fukai and Zhao et al. [15,16] developed a model based on the interface tracking and deforming finite element method to study the deformation of a spherical molten metal droplet impinging on a flat surface. They examined the effects of the impact velocity, droplet diameter, surface tension, and material properties on deforming processes. Waldvogel and Poulikakos [4] investigated the splat morphology and revealed a strong correlation between the fluid dynamics and the solidification behavior of the droplet. Pasandideh-Fard et al. [17–19] simulated the spreading and solidification of tin droplets on a stainless steel substrate using a modified SOLA-VOF method. Their prediction of the splat shape matched well with the experimental observation. Tong and Holt [20] studied the effects of thermophysical properties on splat flattening ratio using a VOF-based code for free surface deformation and an enthalpy method for equilibrium solidification in the droplet. Pasandideh-Fard et al. [19] simulated three-dimensional impact and solidification using a 3D VOF model and an enthalpy method. In most models discussed above, equilibrium solidification was assumed and the enthalpy method for solidification has been employed. Though the non-equilibrium features have been investigated by many researchers, it is limited to one-dimensional cases in which the effects of convective transport and the free surface deformation are neglected [21–26].

In this paper, a numerical model based on the VOF scheme is presented that accounts for free surface movement, thermal contact resistance, and fluid instability. A sub-model is developed to include non-equilibrium solidification phenomena at the solid–liquid interface. This sub-model will be incorporated

into the VOF scheme. In the combined model, the free surface location and movement are obtained by the VOF technique and the solidification interface is determined by a one-dimensional rapid solidification model. The numerical model will be applied to thermal spray coating processes. Physical phenomena such as splat morphology, substrate melting and re-solidification will be investigated. Correlations between the process parameters and the splat morphology will be established.

2. Mathematical model

2.1. Fluid flow and heat transfer

Thermal spray processes, like other solidification processes, can be modeled via two different approaches. The first one describes the transport phenomena using different sets of governing equations for each phase. The different sets of governing equations are coupled through the energy balance at the solidification interface. The location of the solid–liquid interface, therefore, has to be determined as a part of the solution. Numerical implementation of this approach requires a quasi-steady approximation for the interface motion, along with an adaptive grid transformation. The second approach, called enthalpy method, describes the transport phenomena using one set of governing equations for the entire region. This is achieved by introducing a new parameter, the mass fraction of the solidified material, f_s. The value of f_s is defined as zero and unity in the control volume containing the liquid and solid, respectively, and between zero and unity in the cell containing the interface. The energy equation is written in terms of enthalpy. The continuum formulation for the entire region eliminates the need for tracking interfaces. However, a local thermal equilibrium approximation is required.

In this paper, we assumed that the melt behaves like a Newtonian fluid; the flow motion is two-dimensional, axi-symmetric (r,z), and laminar; thermophysical properties are invariant to temperature (without buoyancy force); changes in thermal conductivity and heat capacity with phase change are included but the mass densities of the melt and its solid are the same (i.e., no volumetric change upon phase change). Further, the dependence of the interface temperature on concentration is neglected. Since the flow field is dominated by the forced convection due to impact, the coupling between the velocity and temperature fields is very weak. The error introduced is expected to be small. In consideration of these assumptions, the problem is described mathematically by continuum conservation equations for mass, momentum, and energy as follows [27]:

$$\nabla \cdot \vec{u} = 0, \tag{1}$$

$$\frac{\partial \vec{u}}{\partial t} + \nabla \cdot (\vec{u}\vec{u}) = -\nabla P + \nabla \cdot \left(\frac{1}{f_l Re} \nabla \vec{u} \right) + f_l \frac{\kappa}{We} \nabla F, \tag{2}$$

$$\frac{\partial h}{\partial t} + \nabla \cdot \left(\vec{u} h \right) = \nabla \cdot \left(\frac{\lambda}{RePr} \frac{c_l}{c_s} [\nabla h + \nabla (h_s - h)] \right) - \nabla \cdot \left(f_s (h_l - h_s) \left(\vec{u} - \vec{u}_s \right) \right), \tag{3}$$

where $\vec{u}$ is the mass-averaged velocity vector which is defined as $\vec{u} = f_l \vec{u}_l + f_s \vec{u}_s$ with f_l and f_s being the mass fractions of the liquid and the solid, respectively; κ is the local curvature of the free surface [11]. The governing equations (1)–(3) are non-dimensionalized using the following variables:

$$\begin{aligned} &(x,r) = (x^*, r^*)/b, \quad (u,v) = (u^*, v^*)/U, \quad t = t^* U/b \\ &P = P^*/(\rho U^2), \quad h = (h^* - c_s T_m)/h_f, \\ &\theta = (T - T_m)/(T_p - T_m). \end{aligned} \tag{4}$$

It should be noted that as the densities of the two phases are assumed to be equal, the mass fractions of the phases are identical to their corresponding volume fractions. Also, the substrate velocity has been introduced to account for the effects of the substrate movement on the splat morphology. The last term in Eq. (2) represents the surface tension force concentrated at the free surface. These equations show that the problem is characterized by the *Re*, *Pr*, and *We* numbers, ratio of specific heat between two phases c_l/c_s, and ratio of thermal conductivity of the continuum to that of the liquid $\lambda = (f_s k_s + f_l k_l)/k_l$. The equation of energy, Eq. (3), is expressed in terms of the continuum enthalpy h, defined as

$$h = h_s + f_l (h_l - h_s). \tag{5}$$

The enthalpy for each phase is related to temperature by

$$h_s = c_s (T - T_m)/h_f, \quad h_l = c_l (T - T_m)/h_f + 1. \tag{6}$$

The mass fraction of the liquid is defined as

$$f_l = \begin{cases} 0 & h \leqslant 0, \\ h & 0 < h < 1, \\ 1 & h \geqslant 1. \end{cases} \tag{7}$$

Dimensionless initial conditions for enthalpy are then expressed as follows:

$$h = -Ja \quad \text{for the substrate,} \tag{8}$$

and

$$h = 1 + St \quad \text{for the droplet,} \tag{9}$$

where *Ja* and *St* are the Jakob and Stefan numbers, respectively.

2.2. Rapid solidification

It is understood that the distinguishing feature of rapid solidification in thermal spraying results from non-equilibrium phase transformation with a large melt undercooling and a high solidification rate. The importance of the non-equilibrium kinetics in rapid solidification has stimulated extensive research in this area, and significant progress has been made in developing and understanding the transport phenomena underlying rapid solidification. In the classical equilibrium solidification model, the interface is defined at the location where temperature is at the freezing point of a material, and the rate of solidification is controlled by heat flux balance at the interface. This treatment, however, does not include the undercooling phenomena, which is of great importance to rapid solidification processes during thermal spray coating. It is believed that a substantial undercooling is present in the beginning of the freezing process, and it diminishes as the solidification proceeds [28]. To consider the kinetic effect during rapid solidification, the correlation between the undercooling and the rate of solidification is required. The linear relationship,

$$V_{\mathrm{i}} = \mu_{\mathrm{k}}(\theta_{\mathrm{m}} - \theta_{\mathrm{i}}), \tag{10}$$

has been widely used, where μ_{k} is the linear kinetics coefficient, and θ_{m} and θ_{i} are the equilibrium freezing temperature and the actual interface temperature, respectively. The term, $\theta_{\mathrm{m}} - \theta_{\mathrm{i}}$, is the undercooling.

The energy balance condition at the solidification interface is expressed as follows:

$$\frac{\partial s}{\partial t} = \frac{St}{Pr}\left(\nabla\theta_l - \frac{k_{\mathrm{s}}}{k_{\mathrm{l}}}\nabla\theta_{\mathrm{s}}\right)\cdot\nabla_s, \tag{11}$$

where $s(r,t)$ is the thickness of the solidified layer.

Due to the imperfect contact between the droplet and the substrate, a thermal contact resistance exists. The boundary condition between deposit and substrate can be written as

$$\frac{\partial\theta}{\partial n} = Bi_{\mathrm{c}}(\theta_{\mathrm{B}} - \theta_{\mathrm{sub,i}}) \tag{12}$$

where θ_{B} and $\theta_{\mathrm{sub,i}}$ are the droplet and substrate temperatures at the interface between deposit and substrate, respectively. $Bi_{\mathrm{c}} = h_{\mathrm{c}}d/k$ is the Biot number. For simplicity, a constant heat transfer coefficient $h_{\mathrm{c}} = 5\times 10^7$ W m^{-2} K is used to quantify contact resistance. It is noted that the thermal contact resistance, in reality, is a function of the impacting velocity, surface roughness, and wetting ability, and it changes during the processes. The substrate temperature far away from the deposit, θ_{sub}, is assumed to be constant. An adiabatic thermal condition is applied to the surface of the droplet and the top surface of the substrate, and the initial conditions are $\theta = \theta_{\mathrm{p}}$ for the droplet and $\theta = \theta_{\mathrm{sub}}$ for the substrate.

3. Numerical method

In this section, a numerical scheme is proposed to handle two types of moving interface problems: one is the solidification movement in a splat without substrate melting; and the other is the melting and re-solidification in the substrate without splat solidification. Both cases involve only one moving interface. The fluid dynamics and the free surface deformation are predicted by a modified VOF method [6]. The fractional volume of fluid function, F, is defined to be unity in any control volume fully occupied by fluid, zero in any control volume occupied by void, and between zero and unity in any control volume containing the free surface. The transport equation of the VOF function F can be written as follows:

$$\frac{\partial F}{\partial t} + \nabla\cdot(\vec{u}F) = 0. \tag{13}$$

The enthalpy equation (3) is solved for the entire computational domain and the temperature is then obtained from Eqs. (5) and (6). The enthalpy method assumes local thermal equilibrium. It is, therefore, not suitable to the region where rapid solidification occurs or a local thermal non-equilibrium is present [21,22]. To consider the thermal non-equilibrium, Eqs. (10) and (11) are used instead of Eq. (7) to determine the interface location, the rate of solidification, and the mass fraction of the liquid. Two sets of numerical grids are employed in the simulation. The governing equations are solved using a coarse grid (200×60) for the entire computational domain including the deformable droplet, solidified layer and substrate. When the droplet impacts on the substrate, the energy equation along with the interface conditions (Eqs. (10) and (11)) are solved in the vicinity of the solidification interface (2 μm and 1000 grids on both sides) using a finer mesh to accommodate the rapid solidification. Temperature and enthalpy at the interface will be calculated until the undercooling effect is diminished. The enthalpy at the interface is then used as an internal boundary condition enforced on the control volume containing the interface. In this way, the energy equation is decoupled at the interface so that the rapid solidification model can be applied. The rapid solidification model is solved on a one-dimensional computational domain. The grid size used in the one-dimensional model for solidification is about one hundredth of the typical cell size in the two-dimensional computational domain for the fluid flow model. A time step of 10^{-4} μs is used for solving the freezing problem on the fine grid. This time step is chosen based on grid independent studies. The time step for the fluid flow calculations varies and is determined by instability criteria. The instability criteria in this study are the same as those in Kothe et al. [11]. An additional constraint from solidification was also imposed, which limits the maximum

movement of the interface to a value less than 25% of the grid size for the fluid flow simulation. Since we only deal with droplets impacting on a flat substrate, and consider a very short period of the time when the cooling rate is dominant in the vertical direction, two-dimensional effects will not be significant. In the three-phase contact region, one-dimensional rapid solidification is not applicable. In reality, solidification might not happen immediately in the contact region due to the delay of nucleation. The convection terms are included in the one-dimensional energy equation as source terms. The velocity components, u and v, are obtained using a linear interpolation of the velocities in the two-dimensional coarse grids. The thickness of the coating layer is updated through the rapid solidification model. The shape of the solidification interface can be re-constructed. The mass fraction of the liquid and thermophysical properties is updated, and the fluid field is solved again until the convergent results are achieved.

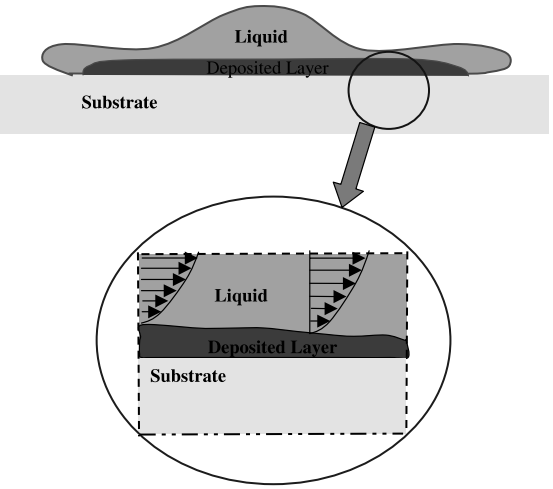

Fig. 1. Schematic of a combined numerical scheme.

4. Results and discussions

4.1. Splat morphology and substrate melting in experiments

The plasma-densified spherical molybdenum powder in the range of 5–44 μm with a mean value of 30 μm (designation SD 152, Osram Sylvania) was used in the experiments. Processing was carried out using a Sulzer Metco PT-F4 plasma gun under an ambient atmosphere. Polished mild steel, sintered molybdenum, and soda lime glass were used as substrates to obtain a wide range of the substrate thermal conductivities. The substrates were placed on the fixture rotating at 160 rpm, 110 mm away from the exit of the torch, and heated by a plasma flame. The substrate temperature was controlled by plasma flame preheating and air-cooling during the deposition, and monitored by an optical pyrometer. The thickness of the mild steel, molybdenum, and glass substrates were 3, 3, and 1.5 mm, respectively. The mild steel and molybdenum substrates were hand-polished to 0.05 μm finishing. The maximum roughness of the substrate surfaces was $Ra = 0.08$ m measured by a Zygo non-contact surface profiler (a scanning white-light interferometer). The glass substrate was not polished due to its highly flat surface finishing. All substrates were cleaned by acetone and dried in air before they were used [29,30]. In-flight particle velocity and temperature was measured by the DPV 2000 system [30] (see Fig. 1).

Fig. 2 shows a typical morphology of molybdenum splats on a mild steel substrate prepared at room temperature. The splats broke into several large fragments. The uneven edge suggested that solidification occurred while the molten droplet was spreading. It is worth mentioning that the image in Fig. 2(a) is similar to the spreading patterns without solidification in Aziz and Chandra [7]. However, the mechanism for the formation of the fragments may be different. The transmission electron microscope (TEM) image of the splat (Fig. 3) shows the existence of an inter-metallic layer between the substrate and splat, which suggests that substrate melting has occurred. The surface topographical measurement reveals that the "valley" between the fragments is lower than the substrate plane (see Fig. 2(b)). Due to the lift-over of the fragments near the outer periphery, the splats look much thicker in the outer periphery than in the central portion. Almost all splats made at room temperature exhibit this feature. The sample prepared at 200°C (see Fig. 2(c)) is a mixture of splashed and disk-shaped splats. Fig. 2(d) shows a typical surface profile of the disk-shaped splats. The morphology of the splats prepared at 400°C is similar to that prepared at 200°C.

Figs. 4(a) and (b) are the morphology of molybdenum splats on molybdenum substrates at room temperature and 340°C, respectively. The room temperature samples show a tendency of fragmentation at the periphery. The splats prepared at 340°C are disk-like, although their rims are not as smooth as those prepared on a hot steel substrate. Splats on the glass substrate are shown in Figs. 4(c) and (d). The splats made at room temperature exhibit fragmented disk shape, with projection along the periphery of the central disk. The splats formed at 340°C display contiguous disk-like shapes with distinguishable rims.

The flattening ratio is defined as a ratio of the splat diameter to the droplet diameter. Due to the difficulty in obtaining uniform size powder in experiments, the average over a range of droplet sizes was taken. This introduced uncertain in the results. In the reported

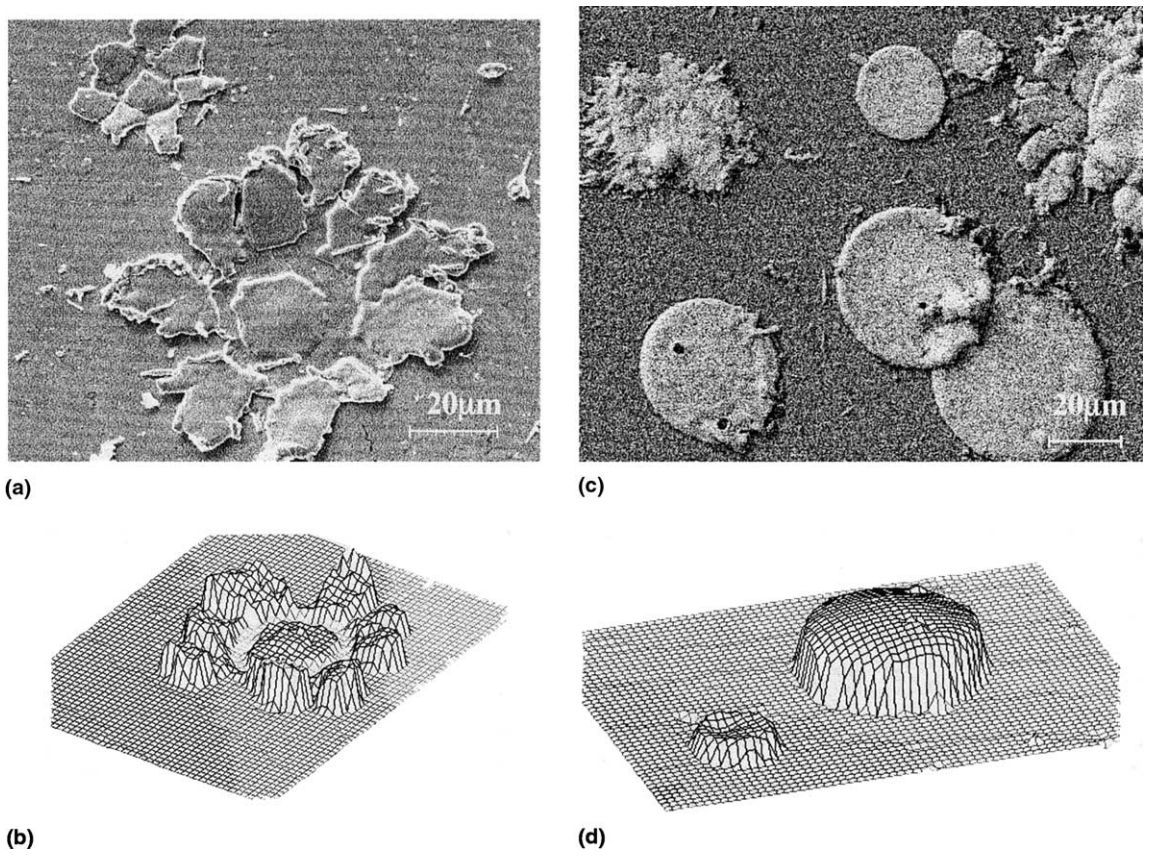

Fig. 2. Molybdenum splats formed on the mild steel substrates and the corresponding 3-D surface profiles (a–b) at room temperature, and (c–d) at 200°C.

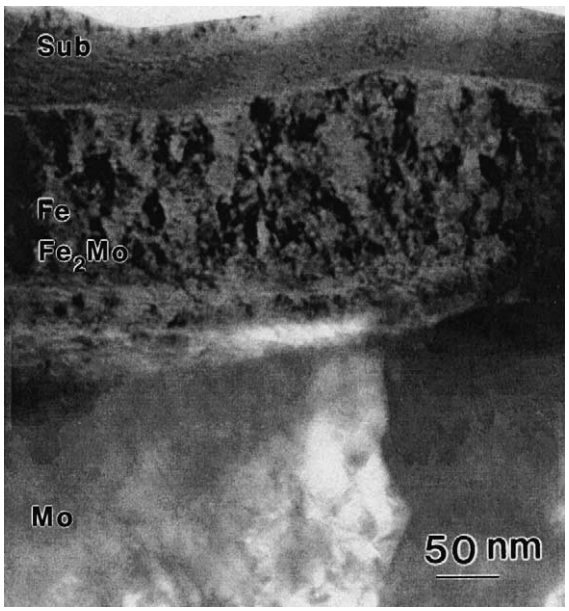

Fig. 3. The TEM photo of a molybdenum splat on a mild steel substrate at room temperature.

experiment, the initial powder size ranges from 5 to 40 μm with an average size of 30 μm. We were able to collect more than 300 splats in one sample. Since the evaporation rates and the trajectories for different sizes of the droplets are different, the final size distribution on the sample could be different. By using a 3-D surface profilometer, the thickness and diameter of the disk-shaped splats formed on a hot substrate were measured, and the volume of the splats and the diameter of the droplet before impact were calculated from these data. The flattening ratio was obtained based on 200 splats ranging from 20 to 40 μm. The initial size distribution, therefore, will not affect the final results. Nevertheless, the uncertainty is present due to the size distribution of the splats. The flattening ratio and the thickness of splats produced on hot steel, molybdenum, and glass substrates are shown in Table 1. The flattening ratio formed on the steel substrate is between 2.0 and 2.8 with an average value of 2.4. The average splat thickness is 2.5 μm. The flattening ratio and the thickness of the splats made on the hot molybdenum substrate are similar to that made on the hot steel substrate. The flattening ratio made on the glass substrate is from 3.0 to 6.5 with an

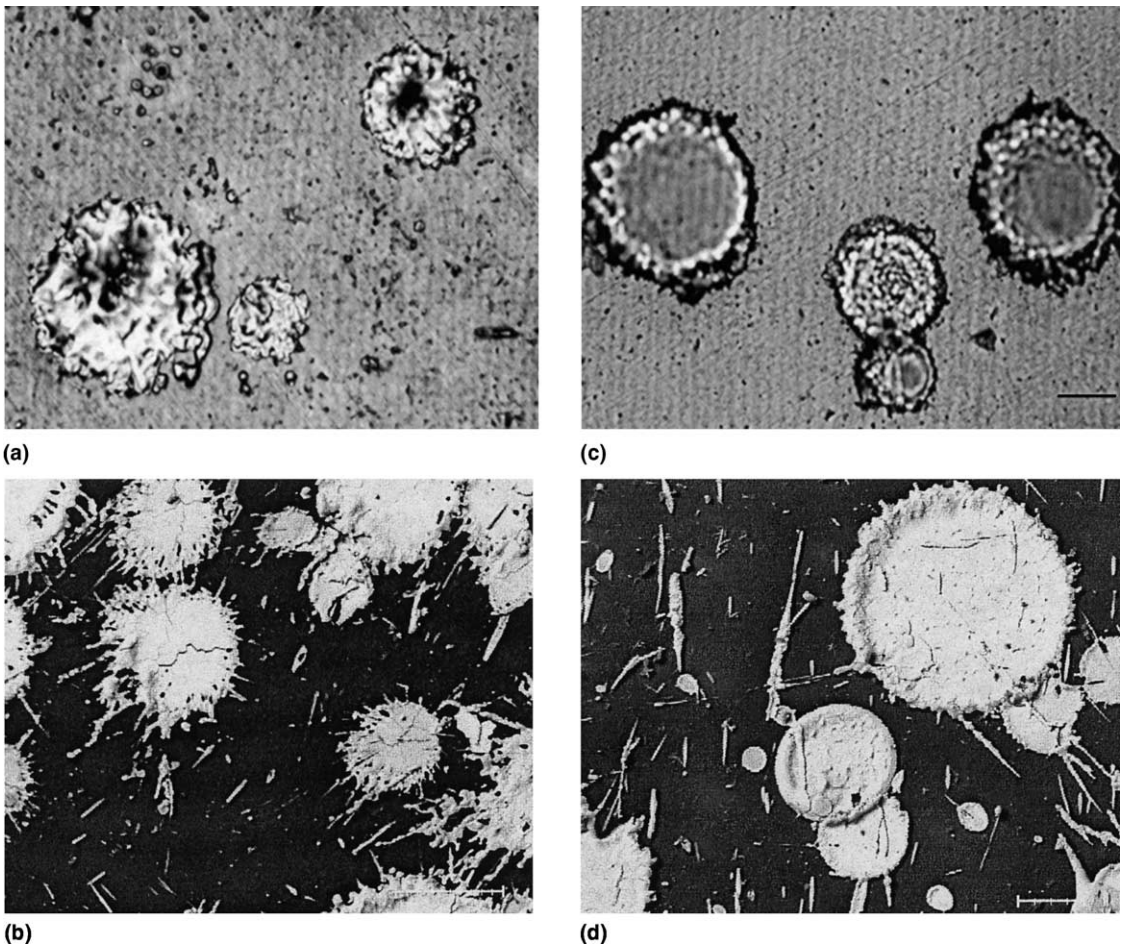

Fig. 4. Molybdenum splats formed on molybdenum substrates (a–b) and glass substrates (c–d) at room temperature (a,c), and 340°C (b,d), respectively.

Table 1
Average particle Reynolds number and estimated splat-flattening ratio

	Mo on Mo	Mo on steel	Mo on glass
Experimental flattening ratio	2.7	2.5	4.6
Experimental splat thickness	2.3 μm	2.5 μm	0.7 μm
Reynolds number	6637	6637	6637
Jakob number based on T_B	1.69	1.55	0.264
Madejski's model, a (ξ)	1.29 (7.50)	1.29 (7.50)	1.29 (7.50)
Wan's model, a (ξ)	0.48 (2.78)	0.48 (2.78)	0.48 (2.78)
Modified model, a (ξ)	0.49 (2.84)	0.50 (2.90)	0.70 (4.07)
Numerical prediction, ξ	2.80	2.80	4.7

average value of 4.5. The average splat thickness is about 0.7 μm [29]. The occurrence of a range of the flattening ratio is not a measurement error, but is rather associated with particle size, temperature and velocity variations as well as the deposition characteristics. The average values of the splat-flattening ratio for three substrates are shown in Table 1.

Fig. 5 displays the effects of the impacting velocity on splat morphology formed on a polished 304 stainless steel substrate at a constant temperature. It is obvious that the droplet velocity has a significant impact on the splat morphology. At a low velocity, disk-shaped splats are obtained. The fragmentation tendency is increased when the droplet velocity increases. It is notable that a

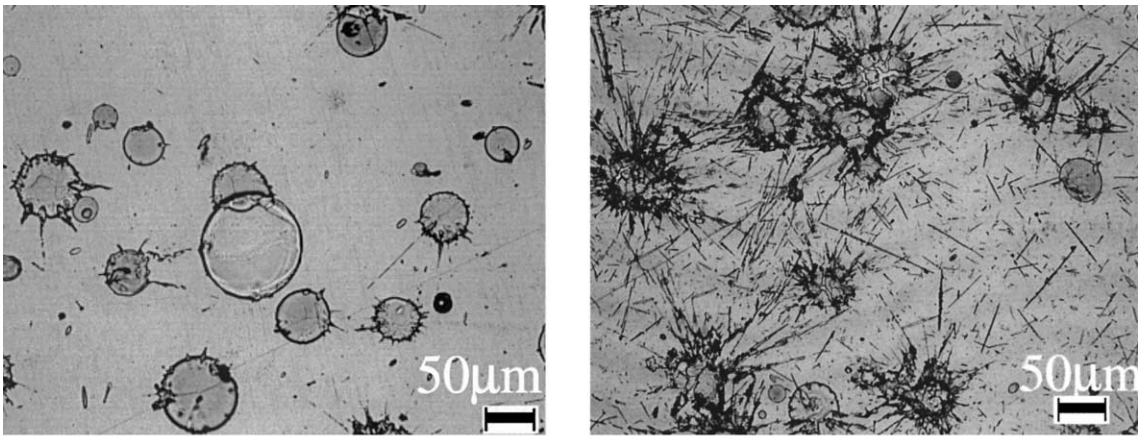

Fig. 5. Effects of the particle velocity on the splat morphology. The impacting velocity is (a) 86 m s^{-1} and (b) 172 m s^{-1}.

few small, disk-shaped splats are formed even though the majority of the splats are fragmented, indicating the dependence of the splat morphology on the droplet size. The experimental results revealed that substrate thermophysical properties, substrate temperature, and droplet velocity affect splat-flattening ratio significantly. A considerable substrate melting occurs for the splats on the steel substrate prepared at room temperature. Although the substrate melting has been known for years, few investigations were performed to examine its influence on splat morphology and adhesion quantitatively.

4.2. Splat flattening ratio

Theoretical models have been developed to correlate the splat-flattening ratio with the particle parameters and the substrate conditions based on the macroscopic mechanical energy balance among the kinetic energy, potential energy, and work done by the frictional force. Madejski [1] concluded that the splat-flattening ratio, ζ, is a function of the Reynolds number, Re, and they are related by

$$\xi = aRe^{0.2}. \tag{14}$$

Modifications were made to Madejski's analysis [3,4,6] to include the effects of the adhesion tension through an equilibrium contact angle defined from the equilibrium solidification. Numerical simulations have also been performed to obtain a better value of the coefficient a. Different values have been obtained by various authors, e.g., $a = 1.2941$ [1], 1.18 [6], 1.04 [12], 1.0 [9], 0.925 [31], 0.83 [32], 0.82 [33]. The experimental results presented earlier indicated that the value of the coefficient a depends strongly on substrate materials. Different values of the splat-flattening ratio can be obtained for the same Reynolds number during molybdenum spreading and solidification (see Table 1). Zhang [6] has derived a theoretical model to correlate the splat-flattening ratio with the spreading, solidification and surface tension. Based on Zhang's model, Wan et al. [34] has obtained a correlation between the splat-flattening ratio and the Reynolds and Jakob numbers by neglecting the surface tension force, which is written as follow:

$$\xi = \left[\sqrt{\frac{Ja}{2Pr}\frac{k_s}{k_l}+1} - \sqrt{\frac{Ja}{2Pr}\frac{k_s}{k_l}}\right]^{0.4}\left(1.18Re^{0.2}\right), \tag{15}$$

where the Jakob number is defined as $Ja = c_l(T_m - T_{sub})/h_f$. Eq. (15) is only true when the substrate temperature remains constant or thermal conductivity of the substrate is much larger than that of the droplet.

To improve the accuracy, Eq. (15) can be further modified to include temperature distribution in the substrate by re-defining the Jakob number based on the temperature difference between the equilibrium freezing temperature, T_m, and the bottom temperature of the droplet, T_B, e.g.,

$$Ja = \frac{c_l(T_m - T_B)}{h_f}. \tag{16}$$

The bottom temperature of the splat can be estimated as

$$T_B = \frac{k_l T_l/\sqrt{\alpha_l} + k_{sub}T_{sub}/\sqrt{\alpha_{sub}}}{k_l/\sqrt{\alpha_l} + k_{sub}/\sqrt{\alpha_{sub}}}. \tag{17}$$

The predictions by all three models proved to be accurate for the case in which the partially stabilized zirconia (PSZ) droplets are deposited on a stainless steel substrate. Because the focus of this paper is on molybdenum droplets, no result on PSZ droplets phenomena is presented. It is pointed out those predictions by Eqs. (14) and (15) differ significantly from the experimental data for the molybdenum on molybdenum, molybdenum on

steel, and molybdenum on glass. For the molybdenum droplets with the size of 30 μm, impinging velocity of 150 m s^{-1}, and temperature of 2883 K, the bottom temperatures of the splats, T_B, for the molybdenum on molybdenum, molybdenum on steel, and molybdenum on glass are 1785, 1877, and 2711 K, respectively. The corresponding Jakob numbers are 1.69, 1.55 and 0.264, respectively. From Eqs. (15)–(17), $a = 0.49$, 0.50, and 0.70 are predicted for the molybdenum on molybdenum, molybdenum on steel, and molybdenum on glass, respectively. The comparison between the predicted flattening ratio and the experimental data is shown in Table 1. The experimental data were obtained based on the average values of 200 splats. It is evident that the flattening ratio for molybdenum on molybdenum is significantly smaller than that for molybdenum on glass, although the particle parameters in both cases are exactly the same. Obviously, the characteristics of substrate materials play an important role in droplet spreading and deposition. The predictions by Eqs. (15)–(17) are in good agreement with the measurements for the flattening ratio of molybdenum on molybdenum and molybdenum on steel, but not molybdenum on glass. Numerical simulation has also been used to predict the values of the flattening ratio using the enthalpy method (Table 1). Results demonstrated that solidification is a two-dimensional process in the case of molybdenum on glass. The prediction from the rapid solidification model is almost the same as that by the enthalpy method. This is simply because the rapid solidification process is much shorter than the time needed to form the disk-shaped splat. Therefore, the splat-flattening ratio may be accurately predicted by the equilibrium solidification model. Due to the size distribution of the droplets, the uncertainty is inevitable in the experimental data of the flattening ratio. Assuming the flattening ratio is proportional to $Re^{0.2}$ and droplet velocities are independent of their sizes, a maximum error of 8% will be introduced for the flattening ratio for the size distribution varying from 20 to 40 μm.

4.3. Substrate melting and re-solidification

Numerical simulations have been performed to study the substrate melting and re-solidification processes. Three substrate materials, molybdenum, mild steel, and glass, have been considered in this study. Correspondent thermophysical properties are listed in Table 2. The molybdenum droplet size used in the parametric study is 30 μm, and the velocity is 150 m s^{-1}. The reference length and the velocity are $b = 2$ μm and $v = 150$ m s^{-1}, respectively.

The characteristics of the melting and re-solidification of a substrate can be better understood by examining the displacement and the velocity of the solid–liquid interface. Fig. 6 shows the solid–liquid interface location as a function of time for a molybdenum droplet deposited on a steel substrate with five droplet temperatures from superheating to undercooling. After a delay necessary to heat the substrate, the substrate starts to melt and the interface moves towards the substrate. After the maximum melting depth is reached, the melt will be re-solidified to the top surface of the substrate. The higher the droplet temperature is, the deeper the substrate will melt.

Neglecting the melting and re-solidification of the substrate, the droplet temperature decreases as soon as the droplet hits the substrate. The rate of solidification is presented in Fig. 7 as a function of the substrate temperature. It is evident that the molybdenum splats complete the solidification at the time ranging from 0.19 μs for a 200 K undercooled droplet to 0.31 μs for a 200 K superheated droplet. The substrate remains in the liquid phase from 0.25 s to 0.75 μs after droplet impacting, as shown in Fig. 6. This reveals that the splat may actually solidify on the molten substrate. This phenomenon explains the good bonding and the formation of the inter-metallic layer in Fig. 4. Different morphologies can be achieved for different impinging temperature conditions. Note that the rate of solidification decreases with time, and it is significantly affected by the initial impacting temperature.

Table 2
Thermophysical properties used in the calculations

	Mo	Steel	Ni	Sn^+	Glass
T_m (K)	2883	1788	1788	502	
h_f (J kg^{-1})	3.71×10^5	2.72×10^5	2.92×10^5	6.0×10^4	
k_l (W m^{-1} K^{-1})	46	26	43	31.0	
k_s (W m^{-1} K^{-1})	84	28	74	60.0	1.17
C_{pl} (J kg^{-1} K^{-1})	570	866.67	620	242	
C_{ps} (J kg^{-1} K^{-1})	339	690.82	595	260	900
ρ_l (kg m^{-3})	9350	7700	7900	7000	
ρ_s (kg m^{-3})	10 200	7850	8900	7000	2000
α_l (m^2 s^{-1})	0.86×10^{-5}	0.39×10^{-5}	0.9×10^{-5}	1.83×10^{-5}	
α_s (m^2 s^{-1})	2.43×10^{-5}	0.52×10^{-5}	1.4×10^{-5}	3.29×10^{-5}	6.5×10^{-7}
μ_k (m s^{-1} K^{-1})	0.26	0.01	0.85	0.1 (assumed)	

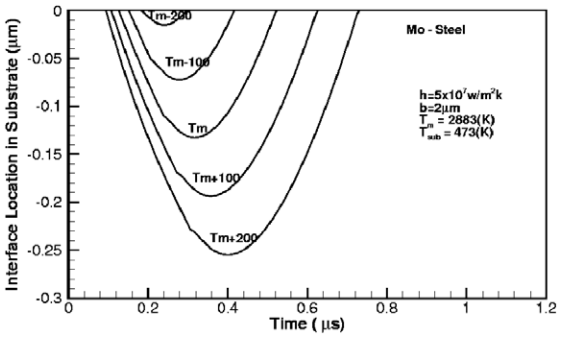

Fig. 6. Melting interface location versus time for molybdenum splats on a steel substrate at the center of the splat.

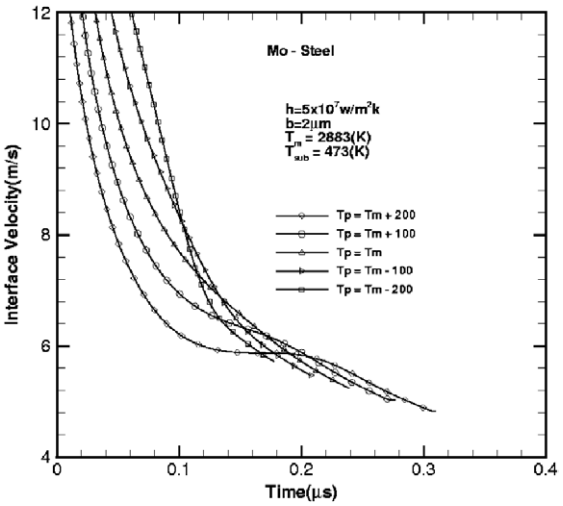

Fig. 7. Solidification interface velocity versus time for molybdenum splats on a steel substrate.

Figs. 8(a)–(c) are the temperature variations on the top and the bottom surfaces of the splat and the top surface of the substrate for molybdenum on steel. Substrate melting has been neglected in the simulation. The maximum substrate temperature at the top surface of the steel substrate is higher than the equilibrium freezing temperature, indicating substrate melting in all three cases. For molybdenum splats on a steel substrate (see Fig. 8(c)), the deepest thickness is achieved due to the highest impacting temperature of the droplet. Variations of the maximum substrate temperature with the substrate and impacting temperatures are shown in Fig. 9 for three types of substrates. It is evident that the characteristics of the substrate material play an important role in substrate melting. For most cases shown in Fig. 9, the maximum temperature is higher than the melting temperature, therefore, the substrate melting and re-solidification will occur. The maximum substrate temperature on a glass substrate is much higher than that on a steel or molybdenum substrate due to a low thermal conductivity of the glass. A flower-like shape of the splats (Fig. 2(a)) forms on the mild steel substrate when the maximum temperature is moderately higher than the melting temperature. For the case where the maximum temperature is much higher than the equilibrium freezing temperature, a disk-shaped splat is observed (Fig. 2(b)). For the Ni splats deposited on a Sn substrate, the experimental observation by Houben [35] revealed that although the melting of the Sn substrate by molten Ni droplets occurred, the flower-like splats were not found. Fig. 8(d) shows the variation of the temperatures on the top and the bottom surfaces of the splat and the top surface of the substrate for Ni droplets deposited on an Sn substrate. The maximum substrate temperature of the top surface is much higher than the freezing temperature of Sn. The Ni droplet will solidify on the molten Sn substrate and a disk-shaped splat is expected.

4.4. Splashed splat morphology

Numerical simulations have been performed to study a molybdenum droplet deposited on a steel substrate. Fig. 10 shows the evolution of the free surface considering substrate melting for a molten molybdenum droplet with the size of 100 μm and velocity of 100 m s^{-1} impacting on a steel substrate. It is found that substrate melting occurs, and the melting pool is limited by the fast cooling of the droplet. The mixing molybdenum/steel molten liquid is jetted out at the edge of the solid substrate. The concentration of the steel has not been solved in this study. The material properties of the mixture have been assumed to be the same as that of the pure molybdenum. The liquid jet detaches the substrate and a splashed splat is obtained. With the increase of the substrate temperature, a larger melting pool of the substrate can be formed, and the droplet will be solidified on the molten substrate. The flower-like splat is not expected.

Fig. 11 shows the simulation results of a splashed splat due to rapid solidification. Substrate melting has been neglected in this case. The rate of solidification is faster than the rate of deformation of the free surface. A thin liquid film with a high shear stress is formed and it is broken into pieces. The splashed splat is shown in Fig. 11(f). It is understood that the splashed splat is due to a high rate of solidification.

5. Conclusion

The splat morphology and substrate melting and re-solidification have been studied numerically and experimentally for molybdenum droplets impacting on

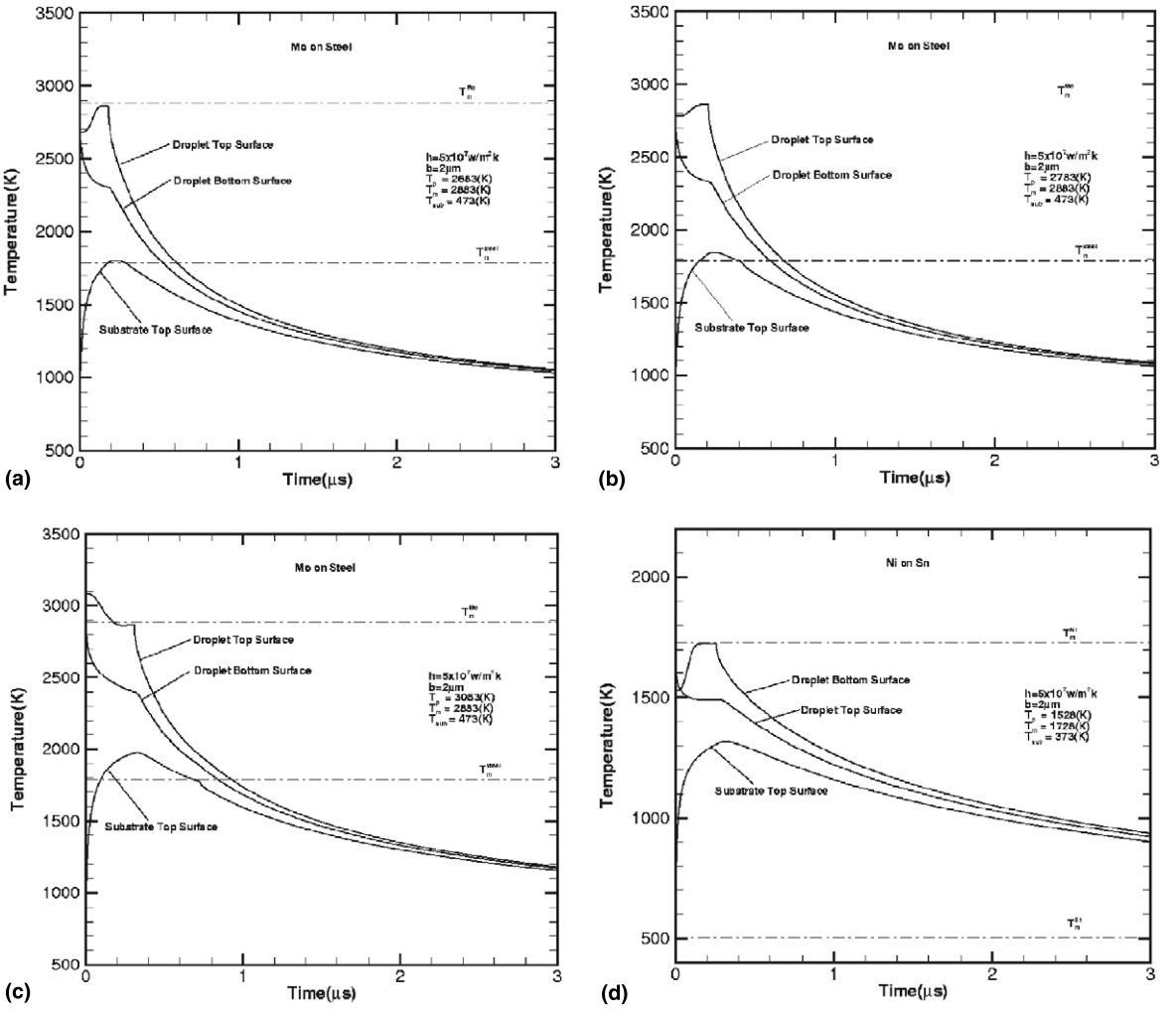

Fig. 8. Temperature versus time when $T_{sub} = 473$ K and (a) $T_p = T_m - 200$ K, (b) $T_p = T_m - 100$ K, (c) $T_p = T_m + 200$ K for molybdenum splats on a steel substrate, and (d) $T_{sub} = 373$ K and $T_p = T_m - 200$ K for Ni splats on a Sn substrate.

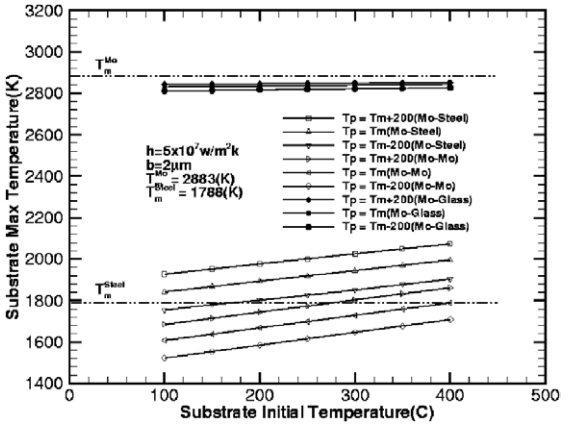

Fig. 9. Maximum substrate temperature versus initial substrate temperature for molybdenum droplets impacting on molybdenum, steel, and glass substrates.

molybdenum, mild steel, and glass substrates. The effects of the droplet size, velocity, temperature, and the substrate material and temperature on the splat morphology and the rate of solidification have been investigated. The correlation between the splat-flattening ratio and the Reynolds and Jakob numbers has been developed. This correlation indicates that substrate melting and re-solidification strongly depends on the impinging temperature of the droplet, substrate temperature, and its thermophysical properties.

Two-dimensional models considering the free surface deformation and rapid solidification have been developed by combining the VOF scheme with either a one-dimensional rapid solidification model or a two-dimensional enthalpy method. The models can predict the rate of solidification, flattening ratio and splat morphology accurately and efficiently. The VOF

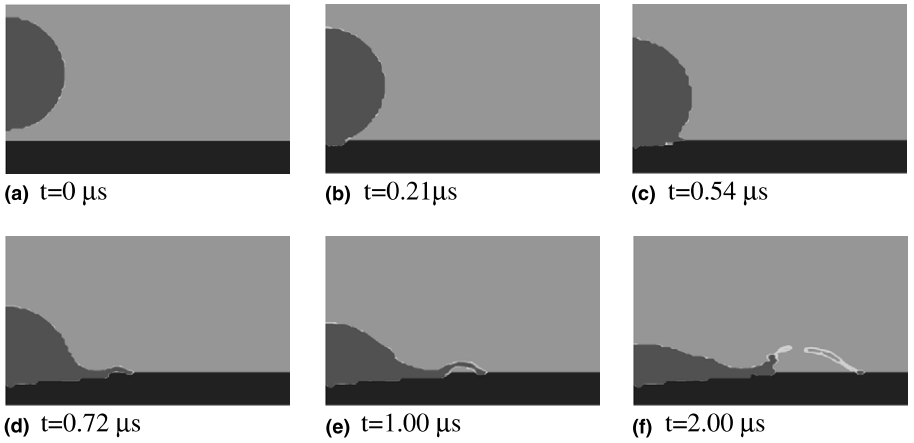

Fig. 10. Free surface evolution and substrate melting of a 100 μm diameter molybdenum droplet impinging on a steel substrate with velocity of 100 m s^{-1}. 200 × 60 non-uniform grids is used (splashing due to substrate melting).

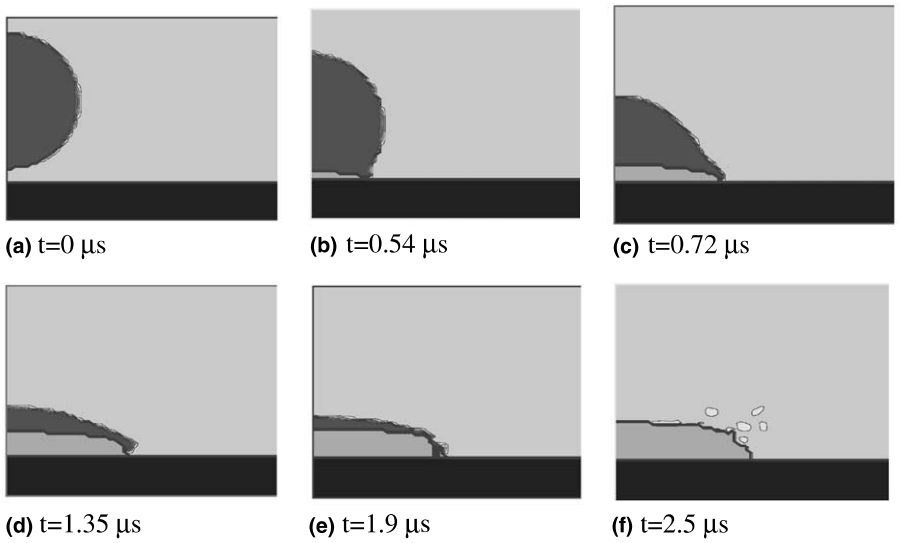

Fig. 11. Free surface evolution and substrate melting of a 100 μm diameter molybdenum droplet impinging on a substrate with velocity of 100 m s^{-1}. 200 × 60 non-uniform grids is used (splashing due to rapid solidification).

scheme combined with the rapid solidification model was used to simulate the rapid solidification of the molybdenum droplets on a mild steel substrate. Simulation results revealed that the droplet and substrate temperatures have significant influences on the melting depth of the substrate and thus on the adhesion of the splat. The maximum substrate temperature is significantly affected by the initial substrate temperature. The results also confirmed that rapid solidification has a significant impact on substrate melting and re-solidification, and the rate of solidification of the splat. The VOF scheme combined with the enthalpy model based on a local thermal equilibrium was used to predict the splat flattening ratio for the molybdenum droplets on molybdenum, mild steel, and glass substrates. The results agree well with the experiments, indicating that rapid solidification is not important whenever a disk-shaped splat is formed.

Acknowledgements

This work was supported by the National Science Foundation under the grants no. CTS-9876198 and CTS-0074589. Acknowledgements are also due to Y.P. Wan of GT Equipment Technologies, Inc., and G.X. Wang of Akron University for helpful discussions and to R. Goswami for the TEM picture.

References

[1] J. Madejski, Solidification of droplets on a cold surface, Int. J. Heat Mass Transfer 19 (1976) 1009–1013.

[2] E.W. Collings, A.J. Markworth, J.K. McCoy, J.H. Saunders, Splat-quench solidification of freely falling liquid-metal drops by impact on a planar substrate, J. Mater. Sci. 25 (1990) 3677–3682.

[3] T. Bennett, D. Poulikakos, Splat-quench solidification: estimating the maximum spreading of a droplet impacting a solid surface, J. Mater. Sci. 28 (1993) 963–970.

[4] J.M. Waldvogel, D. Poulikakos, Solidification phenomena in picoliter size solder droplet deposition on a composite substrate, Int. J. Heat Mass Transfer 40 (1997) 295–309.

[5] J.-P. Delplanque, R.H. Rangel, An improved model for droplet solidification on a flat surface, J. Mater. Sci. 32 (1997) 1519–1530.

[6] H. Zhang, Theoretical analysis of spreading and solidification of molten droplet during thermal spray deposition, Int. J Heat Mass Transfer 42 (1999) 2499–2508.

[7] S.D. Aziz, S. Chandra, Impact, recoil and splashing of molten metal droplets, Int. J. Heat Mass Transfer 43 (2000) 2841–2857.

[8] M. Fukumoto, Y. Huang, Flattening mechanism in thermal sprayed nickel particle impinging on flat substrate surface, J. Therm. Spray Technol. 8 (3) (1999) 427–432.

[9] G. Trapaga, J. Szekely, Mathematical modeling of the isothermal impingement of liquid droplets in spraying processes, Metall. Trans. 22B (1991) 901–914.

[10] G. Trapaga, E.F. Matthys, J.J. Valencia, J. Szekely, Fluid flow, heat transfer, and solidification of molten metal droplets impinging on substrates: comparison of numerical and experimental results, Metall. Trans. 23B (1992) 701–718.

[11] D.B. Kothe, R.C. Mjolsness, M.D. Torrey, RIPPLE: a computer program for incompressible flows with free surfaces, Los Alamos National Lab. Technical report LA-12007-MS, Los Alamos, New Mexico, 1991.

[12] H. Liu, E.J. Lavernia, R.H. Rangel, Numerical simulation of impingement of molten Ti, Ni, and W droplets on a flat substrate, J. Therm. Spray Technol. 2 (1993) 369–378.

[13] H. Liu, E.J. Lavernia, R.H. Rangel, Modeling of molten droplet impingement on a non-flat surface, Acta Metall. Mater. 43 (1995) 2053–2072.

[14] X. Bian, J.-P. Delplanque, R.H. Rangel, Droplet deposition: comparison of models, numerical simulation and experimental results, in: Proceedings of the 32nd National Heat Transfer Conference of ASME, New York, NY, HTD-Vol. 347, 1997, pp. 75–82.

[15] J. Fukai, Y. Shiiba, T. Yamamoto, O. Miyatake, D. Poulikakos, C.M. Megaridis, Z. Zhao, Wetting effects on the spreading of a liquid droplet colliding with a flat surface: experiment and modeling, Phys. Fluids 7 (1995) 236–247.

[16] Z. Zhao, D. Poulikakos, J. Fukai, Heat transfer and fluid dynamics during the collision of a liquid droplet on a substrate-I. Modeling, Int. J. Heat Mass Transfer 39 (1996) 2771–2789.

[17] M. Pasandideh-Fard, J. Mostaghimi, On the spraying and solidification of molten particles in a plasma spray process: effect of thermal contact resistance, Plasma Chem. Plasma Process. 16 (1996) 83S–98S.

[18] M. Pasandideh-Fard, R. Bhola, S. Chandra, J. Mostaghimi, Deposition of tin droplets on a steel plate: simulations and experiments, Int. J. Heat Mass Transfer 41 (1998) 2929–2945.

[19] M. Pasandideh-Fard, J. Mostaghimi, S. Chandra, On a three-dimensional model of free surface flows with heat transfer and solidification, in: Proceedings of the Third ASME/JSME Joint Fluids Engineering Conference, FEDSM99-7112, San Francisco, 1999, pp. 1–6.

[20] A.Y. Tong, B.R. Holt, Numerical study on the solidification of liquid metal droplets impacting onto a substrate, Numer. Heat Transfer 31 (1997) 797–818.

[21] G.X. Wang, E.F. Matthys, Experimental investigation of interfacial thermal conductance for molten metal solidification on a substrate, J. Heat Transfer 118 (1996) 157–163.

[22] G.X. Wang, E.F. Matthys, Modeling of nonequilibrium surface melting and resolidification for pure metals and binary alloys, J. Heat Transfer 118 (1996) 944–951.

[23] S.P. Wang, G.X. Wang, E.F. Matthys, Melting and resolidification of a substrate in contact with a molten metal: operational maps, Int. J. Heat Mass Transfer 41 (1998) 1177–1188.

[24] S.P. Wang, G.X. Wang, E.F. Matthys, Deposition of a molten layer of high melting point material: substrate melting and resolidification, Mater. Sci. Eng. A262 (1999) 25–32.

[25] C.H. Amon, K.S. Schwaltz, R. Merz, F.B. Prinz, Numerical and experimental investigation of interface bonding via substrate remelting of an impinging molten metal droplet, J. Heat Transfer 118 (1996) 164–172.

[26] K.S. Schmaltz, L.J. Zarzalejo, C.H. Amon, Molten droplet solidification and substrate remelting in microcasting Part II: parametric study and effect of dissimilar material, Heat Mass Transfer 35 (1999) 17–23.

[27] H. Zhang, M.K. Moallemi, S. Kumar, Thermal analysis of the hot dip-coating process, J. Heat Transfer 115 (1993) 453–460.

[28] M. Vardelle, A. Vardelle, A.C. Leger, P. Fauchais, D. Gobin, Influence of particle parameters at impact on splat formation and solidification in plasma spraying processes, J. Therm. Spray Technol. 4 (1994) 50–58.

[29] X.Y. Jiang, J. Matejicek, S. Sampath, Substrate temperature effects on the splat formation, microstructure development and properties of plasma sprayed coatings, Part II: case study for molybdenum, Mater. Sci. Eng. A272 (1999) 189–198.

[30] X.Y. Jiang, Deposit formation dynamics and microstructure development during thermal spraying, Ph.D. dissertation, State University of New York at Stony Brook, NY, 2000.

[31] M. Bertagbnolli, M. Marchese, G. Jacucci, Modeling of particle impacting on a rigid substrate under plasma spraying conditions, J. Therm. Spray Technol. 4 (1995) 41–49.

[32] T. Yoshida, T. Okada, H. Hamatani, H. Kumaoka, Integrated fabrication process or solid oxide fuel cells using novel plasma spraying, Plasma Sources Sci. Technol. 1 (1992) 195–201.

[33] T. Watanabe, I. Kuribayashi, T. Honda, A. Kanzawa, Deformation and solidification of a droplet on a cold substrate, Chem. Eng. Sci. 47 (1992) 3059–3065.

[34] Y.P. Wan, H. Zhang, X.Y. Jiang, S. Sampath, V. Prasad, Role of solidification, substrate temperature and Reynolds number on droplet spreading in thermal spray deposition: measurements and modeling, J. Heat Transfer 123 (2001) 382–389.

[35] J.M. Houben, Future developments in thermal spraying, in: Proceedings of the Second National Conference on Thermal Spray, 1978, pp. 1–19.